Contribution from the Chemistry Department,
Imperial College of Science and Technology, London, SW7 2AY, United Kingdom

Crystal Structures of Dichlorobis(triphenylphosphine oxide)zinc(II) and Dibromobis(triphenylphosphine oxide)zinc(II) and an EPR Study of Manganese(II) in Dibromobis(triphenylphosphine oxide)zinc(II)

CHARLES A. KOSKY,*[1a] JEAN-PIERRE GAYDA,[1b] JOHN F. GIBSON, STEPHEN F. JONES, and DAVID J. WILLIAMS

Received November 30, 1981

The structures of $ZnX_2(OPPh_3)_2$ (X = Cl, Br) have been determined. Crystals of the chloride are orthorhombic, with a = 32.95 (1) Å, b = 20.702 (6) Å, c = 9.792 (3) Å, space group $Fdd2$, and Z = 8; those of the bromide are triclinic, with a = 10.188 (1) Å, b = 9.987 (1) Å, c = 11.189 (1) Å, α = 114.58 (1)°, β = 121.29 (1)°, γ = 89.82 (1)°, space group $P1$, and Z = 1. The environment of the metal atom in each case approximates to a tetrahedral arrangement of two oxygens and two halide ions. A single crystal of the bromide doped with manganese in the zinc site was studied by electron paramagnetic resonance at room temperature, and its spin Hamiltonian parameters are reported, notably **D** = 0.523 cm^{-1} and **E** = 0.133 cm^{-1}. The high value of **D** for the bromide relative to that of the chloride is in keeping with the general observation that **D** increases in the order of Cl < Br < I for a given class of compound, which is also the order of increasing electron release from the ligand. The orientations of the principal values of **D** found for the bromide are used as a basis for assigning their most probable orientations in the chloride, where there are two magnetically independent molecules. We observe that the principal axes of **D** avoid the bond directions, D_x lying along or close to the bisector of the XMnX direction (X = Cl, Br) and D_y and D_z lying close to the OMnX planes (X = Cl, Br). Chlorine, being the more electronegative, more strongly influences the direction of D_y in the chloride than does bromine in the bromide. But in the latter the π-electron density of a phenyl group may be a contributory factor.

Introduction

In spite of the fact that considerable experimental and theoretical work has been performed on multielectron transition-metal ions with a view to measuring the zero-field splitting and to understanding the causes for it, an all-embracing explanation of the pertinent mechanisms that contribute to this splitting is still not universally accepted. Most of the published work refers to oxides, fluorides, and other predominantly ionic compounds doped with S-state ions such as Mn^{2+}, Fe^{3+}, Eu^{2+}, and Gd^{3+}, and although other halide hosts and more covalent compounds have been studied, there is still no large body of experimental data relevant to these classes of compounds. From the data that are available, there is good evidence that overlap and covalent effects do contribute to the ground-state splitting in certain cases as clearly may be anticipated by the finding that **D** consistently increases in the order Cl < Br < I in various series of compounds.[2] Much of the data that do exist for these more covalent lattices have been determined from powders and for various reasons may be unreliable, a point we discuss later. It is for these reasons therefore that we have studied single crystals of a series of manganese-doped zinc compounds $Zn(Mn)(OPPh_3)_2X_2$ (X = Cl, Br, I) in which the d^5 Mn^{2+} ion is approximately tetrahedrally surrounded by two oxygens and two halogens, with a view to measuring the spin Hamiltonian parameters accurately and relating them to the known structures. In an earlier paper[3] we reported such data for the chloride over a temperature range; in this paper we report the bromide at room temperature and the X-ray crystallographically determined structures of both these compounds.

Experimental Section

Materials. $Zn(Mn)Br_2(OPPh_3)_2$. To a mixture of ethanol (60 mL) and HBr (1 mL) was added $ZnBr_2$ (0.004 mol), $MnBr_2 \cdot 4H_2O$ (20 μmol) and Ph_3PO (0.013 mol) with stirring until all the solids dissolved. The solution was refluxed for 2 h, after which cooling to room temperature yielded the white polycrystalline product. This was separated by filtration (2.72 g) and recrystallized from methanol (30 mL) over a period of 3 days to yield transparent tabular crystals.

$Zn(Mn)I_2(OPPh_3)_2$. To ethanol (40 mL) containing a few drops of HI was added with stirring ZnI_2 (0.004 mol), Ph_3PO (0.012 mol), and a few crystals of $MnI_2 \cdot 4H_2O$. After the solution was refluxed for 2 h and cooled, the yellow product was separated by filtration and washed with benzene. A solution containing 0.5 g of this product in ethanol (30 mL) was slowly evaporated, yielding tabular crystals similar in external appearance to those of the dibromo compound.

Crystals of the two pure zinc compounds, i.e., containing no manganese, were similarly prepared for the X-ray crystallographic studies; those of pure $ZnCl_2(OPPh_3)_2$ were available from the earlier work.[3]

Structure Determinations. Crystals of $ZnBr_2(OPPh_3)_2$ are triclinic, with a = 10.188 (1) Å, b = 9.987 (1) Å, c = 11.189 (1) Å, α = 114.58 (1)°, β = 121.29 (1)°, γ = 89.82 (1)°, U = 808.5 $Å^3$, Z = 1, and D_c = 1.61 g cm^{-3}; the space group is $P1$, and μ(Cu Kα) = 52 cm^{-1}.

Data were measured on a Siemens off-line four-circle diffractometer with Ni-filtered Cu Kα radiation. A total of 2543 independent reflections were measured ($\theta \leq 60°$) with the θ–2θ scan technique with the "five-value"[4] measuring routine. Of these, 29 reflections had $I < 2.58\sigma(I)$ and were classed as unobserved.[4] The data were corrected for absorption by using the method of Busing and Levy[5] with crystal path lengths determined by the procedure of Coppens, Leiserowitz, and Rabinovich.[6]

The structure was solved by the "heavy-atom" method, and the non-hydrogen atoms were refined anisotropically. The hydrogen atoms were placed at fixed calculated positions and the structure refined to give R = 0.044. Refinement with the complex component of the anomalous scattering factors (f'') for Zn, Br, and P positive gave R

(1) (a) Present address: Manhattan Community College, City University of New York, New York, NY 10019. (b) Present address: Département d'Electronique, Université de Provence, Centre de St. Jerôme, 13397 Marseille, France.

(2) (a) Birdy, R. B.; Goodgame, M. *Inorg. Chim. Acta* **1981**, *56*, 181. (b) Birdy, R. B. Ph.D. Thesis, University of London, 1977. (c) Rivera, J.-P.; Bill, H.; Weber, J.; Lacroix, R.; Hochstrasser, G.; Schmid, H. *Solid State Commun.* **1974**, *14*, 21. (d) Cotton, S. A.; Gibson, J. F. *J. Chem. Soc. A* **1971**, 859, 1696. (e) Dowsing, R. D.; Gibson, J. F.; Goodgame, M.; Hayward, P. J. *J. Chem. Soc. A* **1969**, 187; **1970**, 1133. (f) Dowsing, R. D.; Gibson, J. F.; Goodgame, D. M. L.; Goodgame, M.; Hayward, P. J. *J. Chem. Soc. A* **1969**, 1242. (g) Heming, M.; Lehmann, G. *Chem. Phys. Lett.* **1981**, *80*, 235.

(3) Vivien, D.; Gibson, J. F. *J. Chem. Soc., Faraday Trans. 2* **1975**, *71*, 1640.

(4) Allen, F. H.; Rogers, D.; Troughton, P. G. H. *Acta Crystallogr., Sect. B* **1971**, *B27*, 1325.

(5) Busing, W. R.; Levy, H. A. *Acta Crystallogr.* **1957**, *10*, 180.

(6) Coppens, P.; Leiserowitz, L.; Rabinovich, D. *Acta Crystallogr.* **1965**, *18*, 1035.

0020-1669/82/1321-3173$01.25/0

Table I. Fractional Atomic Coordinates (×10⁴) for $ZnBr_2(OPPh_3)_2$ with Estimated Standard Deviations in Parentheses

atom	x	y	z
Zn	0	0	0
Br(1)	2695 (2)	510 (2)	2040 (2)
Br(2)	−1669 (2)	−2445 (1)	−1221 (2)
P(1)	578 (3)	483 (3)	−2479 (3)
P(2)	−1208 (3)	3171 (3)	1188 (3)
O(1)	−279 (8)	143 (9)	−1813 (8)
O(2)	−901 (8)	1640 (7)	754 (8)
C(111)	2129 (11)	−460 (10)	−2223 (10)
C(121)	−878 (12)	−293 (11)	−4588 (11)
C(131)	1324 (11)	2468 (10)	−1672 (11)
C(211)	507 (12)	4717 (12)	2173 (12)
C(221)	−1845 (11)	3622 (11)	2519 (11)
C(231)	−2795 (12)	3204 (11)	−572 (12)
C(112)	3512 (12)	148 (12)	−2032 (13)
C(113)	4596 (13)	−701 (13)	−1938 (14)
C(114)	4377 (14)	−2070 (14)	−2005 (13)
C(115)	3022 (15)	−2661 (14)	−2191 (15)
C(116)	1920 (13)	−1793 (12)	−2261 (14)
C(122)	−2470 (13)	−730 (13)	−5213 (14)
C(123)	−3637 (19)	−1271 (17)	−6794 (18)
C(124)	−3185 (25)	−1454 (19)	−7785 (19)
C(125)	−1642 (24)	−1071 (19)	−7264 (18)
C(126)	−440 (16)	−469 (16)	−5615 (14)
C(132)	506 (13)	3261 (12)	−2405 (14)
C(133)	975 (14)	4853 (13)	−1665 (15)
C(134)	2341 (15)	5663 (14)	−134 (15)
C(135)	3194 (14)	4861 (13)	622 (14)
C(136)	2718 (13)	3295 (12)	−75 (12)
C(212)	418 (15)	5957 (13)	1960 (16)
C(213)	1761 (19)	7204 (16)	2865 (19)
C(214)	3194 (18)	7125 (17)	4001 (18)
C(215)	3322 (15)	5861 (17)	4201 (15)
C(216)	1995 (14)	4621 (14)	3318 (13)
C(222)	−1630 (14)	5066 (12)	3554 (13)
C(223)	−2211 (15)	5365 (14)	4512 (14)
C(224)	−3010 (14)	4134 (14)	4342 (14)
C(225)	−3239 (15)	2671 (14)	3314 (15)
C(226)	−2666 (14)	2369 (12)	2367 (13)
C(232)	−2918 (15)	2409 (16)	−1975 (14)
C(233)	−4150 (19)	2358 (19)	−3364 (17)
C(234)	−5234 (18)	3171 (18)	−3326 (16)
C(235)	−5148 (16)	3948 (16)	−1961 (17)
C(236)	−3926 (14)	4018 (13)	−549 (14)

= 0.042; refinement with f'' negative gave $R = 0.045$. Refinement was terminated at $R = 0.042$.

Crystals of $ZnCl_2(OPPh_3)_2$ are orthorhombic, with $a = 32.95$ (1) Å, $b = 20.702$ (6) Å, $c = 9.792$ (3) Å, $U = 6679$ Å^3, space group $Fdd2$, $Z = 8$, $D_c = 1.38$ g cm^{-3}, and μ(Cu Kα) = 37 cm^{-1}.

Data were measured with use of monochromatised Cu Kα radiation (graphite monochromator) on a Nicolet R3m diffractometer. A total of 1125 independent reflections were measured ($\theta \leq 55°$) with the ω-scan measuring routine, and of these 14 had $F_o < 3\sigma(F_o)$ and were classed as unobserved. The data were corrected for absorption with an empirical correction based on 310 psi measurements. The structure was solved by refining the coordinates for the closely isostructural $CuCl_2(OPPh_3)_2$ compound.[7] The non-hydrogen atoms were refined anisotropically; the hydrogen atoms were placed at calculated positions and allowed to ride on their parent carbon atoms. Refinement was terminated at a final $R = 0.043$.

Computations for the bromide were carried out on the Imperial College CDC 6500 and the University of London CDC 7600 computers with in the main, programs belonging to the X-RAY 72 system. Those for the chloride were carried out on an Eclipse S140 computer with the SHELXTL program system. Scattering factors and anomalous scattering factors were taken from ref 8.

Fractional atomic coordinates for the non-hydrogen atoms, together with their estimated standard deviations for the bromide and chloride, are given in Tables I and II, respectively. Table III gives the comparative geometries for the tetrahedra and the phosphorus atoms.

(7) Bertrand, J. A.; Kalyanaraman, A. R. *Inorg. Chim. Acta* **1971**, *5*, 341.
(8) "International Tables for X-ray Crystallography"; Kynoch Press: Birmingham, England, 1974; Vol. IV.

Table II. Fractional Atomic Coordinates (×10⁴) for $ZnCl_2(OPPh_3)_2$ with Estimated Standard Deviations in Parentheses

atom	x	y	z
Zn	0	0	10000
Cl	−306 (1)	759 (1)	11163 (3)
P	702 (1)	835 (1)	8193 (2)
O	385 (1)	361 (2)	8669 (5)
C(11)	1160 (2)	755 (3)	9228 (8)
C(12)	1243 (2)	180 (3)	9866 (10)
C(13)	1584 (2)	123 (4)	10673 (10)
C(14)	1845 (2)	625 (4)	10848 (9)
C(15)	1769 (2)	1203 (4)	10199 (9)
C(16)	1425 (2)	1276 (4)	9401 (9)
C(21)	811 (2)	702 (3)	6452 (7)
C(22)	535 (3)	352 (5)	5690 (10)
C(23)	581 (4)	282 (8)	4295 (14)
C(24)	922 (3)	533 (6)	3682 (11)
C(25)	1202 (3)	846 (5)	4399 (11)
C(26)	1146 (2)	943 (4)	5805 (9)
C(31)	547 (2)	1661 (3)	8395 (7)
C(32)	447 (2)	2040 (3)	7267 (9)
C(33)	327 (2)	2667 (4)	7414 (11)
C(34)	300 (2)	2932 (3)	8704 (11)
C(35)	389 (2)	2575 (4)	9845 (10)
C(36)	513 (2)	1925 (3)	9695 (8)

Table III. Distances (Å) and Angles (Deg) around the Zinc Tetrahedron in $ZnCl_2(OPPh_3)_2$ and $ZnBr_2(OPPh_3)_2$, with Estimated Standard Deviations in Parentheses

	$ZnBr_2(OPPh_3)_2$		$ZnCl_2$-$(OPPh_3)_2$
	Distances		
Zn-Br(1)	2.354 (1)	Zn-Cl	2.187 (2)
Zn-Br(2)	2.357 (2)		
Zn-O(1)	1.965 (10)	Zn-O	1.967 (5)
Zn-O(2)	1.970 (8)		
O(1)-P(1)	1.523 (12)	O-P	1.507 (5)
O(2)-P(2)	1.486 (8)		
	Angles		
Br(1)ZnBr(2)	116.6 (1)	ClZnCl′	117.2 (1)
Br(1)ZnO(1)	113.1 (2)	ClZnO	111.7 (1)
Br(1)ZnO(2)	110.1 (2)		
Br(2)ZnO(1)	103.3 (2)	Cl′ZnO	108.7 (1)
Br(2)ZnO(2)	111.6 (2)		
O(1)ZnO(2)	100.9 (4)	OZnO′	97.0 (3)
ZnO(1)P(1)	145.0 (4)	ZnOP	154.1 (3)
ZnO(2)P(2)	157.0 (7)		
	Dihedral Angle		
[O(1)ZnO(2)]-[Br(1)ZnBr(2)]	85.7	[OZnO′]-[ClZnCl′]	87.8

Tables of other bond lengths and angles, hydrogen atom coordinates, and anisotropic thermal parameters are available as supplementary material.

EPR Measurements. EPR measurements were carried out at X band (~9.2 GHz) with a Varian E12 spectrometer and at Q band (~36 GHz) with a Varian microwave bridge and cavity combined with a Newport Instruments 12-in. Type F electromagnet powered by a C905 rotary generator. In each case the field was calibrated with proton or lithium nuclear magnetic resonance.

For X-band measurements crystals were mounted with grease on a Teflon block stuck with wax to a Teflon plate. The plate was supported by a short horizontal copper wire about which it could be rotated through approximately 70° by means of fine nylon wires attached to its ends. The 70° in situ variable rotation was insufficient for some purposes. When this was the case, a further 90° fixed rotation was obtained by turning the block and refixing it to the plate. The whole of this assembly was held in the cavity by a conventional goniometer, which permitted rotations about a vertical axis.

These two independent rotations permitted any crystal direction within a hemisphere to be brought into alignment with the laboratory magnetic field direction. The horizontal (H) and vertical (V) rotations required to do this were noted and transferred to a stereogram so that

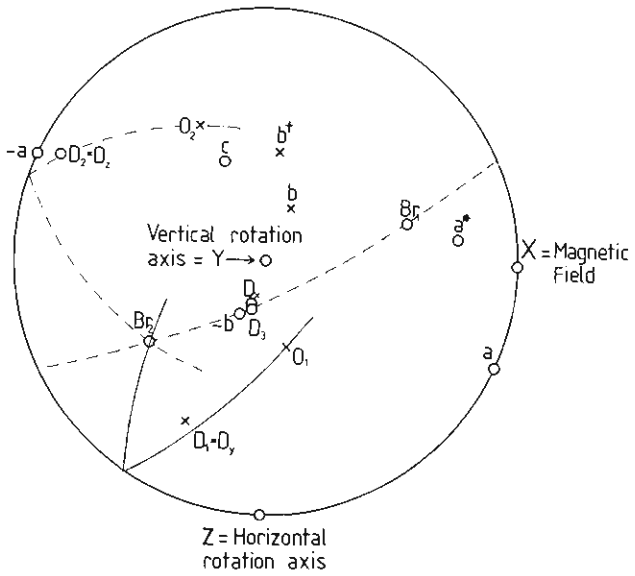

Figure 1. Stereographic projection of the situation at the start of the experiment before any horizontal or vertical rotations around the crystal-mount axes. The zinc (manganese) atom is at the center. Vectors piercing the upper hemisphere are represented as circles and those piercing the lower hemisphere as crosses.

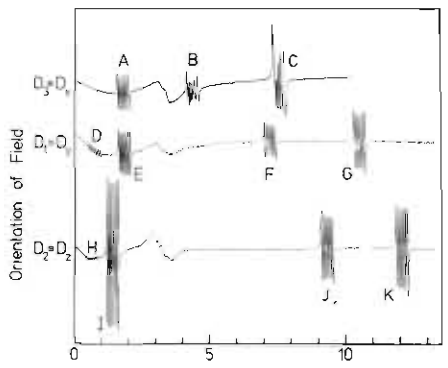

Figure 2. X-Band spectra (9.515 GHz) of $Zn(Mn)Br_2(OPPh_3)_2$ with field along the three principal axes of the **D** tensor found experimentally as D_1, D_2, and D_3 and assigned to D_y, D_z, and D_x, respectively, of the Hamiltonian in ref 3 (label for horizontal axis should read field/kG).

the directions of interest (**D**-tensor principal axes) could be related to the crystalline, and hence the molecular, axes. Unfortunately, the apparatus was too large for the quartz insert of a variable-temperature accessory so only room-temperature measurements were possible. For Q-band measurements crystals were mounted on specially cut Teflon wedges.

A sufficiently large crystal of the $Zn(Mn)Br_2(OPPh_3)_2$ compound (2 mm × 2 mm × 1 mm) was selected to ensure a good signal to noise ratio for the EPR work. The principal crystallographic directions in this crystal were identified by means of Weissenberg and precession photographs and related to the morphology of the crystal, which was sufficiently large that crystallographic axes could be recognized by the naked eye for the purpose of mounting in the spectrometer. The corresponding iodide crystals always revealed splitting of the diffraction spots in their zero-layer Weissenberg photographs, indicative of twinning, so the corresponding manganese-doped single-crystal EPR study was abandoned.

Stereographic Projection. In order to record the experimental EPR data and refer it to the crystallographic axes and molecular bond directions, we used a stereographic net. A set of laboratory axes, X, Y, Z, was chosen to represent respectively the magnetic field direction and the vertical and horizontal axes of rotation. These are orthogonal at the beginning of the experiment but not after the first rotation about the vertical axis. By observation of the crystal under a microscope the orientation of the crystallographic set of axes relative to X, Y, Z was estimated and these two sets of axes were plotted on the stereogram of Figure 1.

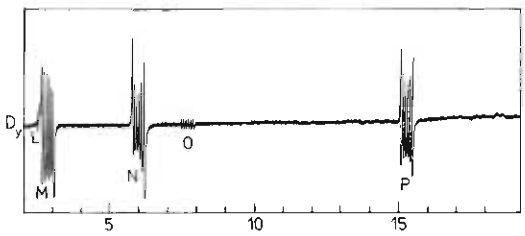

Figure 3. Q-Band spectrum (35.55 GHz) of $Zn(Mn)Br_2(OPPh_3)_2$ with field close to the D_y principal axis. (label for horizontal axis should read field/kG).

Table IV. X-Band (9.515 GHz) Single-Crystal EPR Spectrum of $Zn(Mn)Br_2(OPPh_3)_2$

designation in Figure 2	magnetic field orientation	magnetic field[a] exptl	magnetic field[a] calcd[b]	transition	calcd[b] transition probability
A	$B \parallel x$	1680	1665	$^5/_2$ ($-^3/_2$) → $^3/_2$, $-^5/_2$ ($^1/_2$)	5.78
B	$B \parallel x$	4204	4224	$^1/_2$, $-^3/_2$ ($^5/_2$) → $-^5/_2$, $-^1/_2$ ($^3/_2$)	0.53
C	$B \parallel x$	7463	7525	$^5/_2$, $^1/_2$ ($-^3/_2$) → $^3/_2$ ($-^1/_2$)	18.5
D	$B \parallel y$	729	715	$^5/_2$ ($^1/_2$) → $-^5/_2$ ($-^1/_2$)	0.22
E	$B \parallel y$	1807	1808	$^3/_2$ ($-^1/_2$) → $-^3/_2$ ($^1/_2$)	6.06
F	$B \parallel y$	7176	7152	$^3/_2$, $-^1/_2$ ($-^5/_2$) → $^5/_2$ ($-^3/_2$, $-^1/_2$)	4.47
G	$B \parallel y$	10474	10472	$^5/_2$ ($^1/_2$, $-^3/_2$) → $-^1/_2$ ($^3/_2$)	3.81
H	$B \parallel z$	688	685	$^5/_2$ ($^1/_2$) → $-^5/_2$ ($-^1/_2$)	0.06
I	$B \parallel z$	1453	1430	$^3/_2$ ($-^1/_2$) → $-^3/_2$ ($^1/_2$)	4.35
J	$B \parallel z$	9340	9348	$-^5/_2$ ($-^1/_2$) → $^1/_2$ ($-^3/_2$)	3.22
K	$B \parallel z$	12100	12097	$^1/_2$ ($-^3/_2$) → $-^5/_2$ ($-^1/_2$)	3.57

[a] In Gauss. [b] Using data presented in Table VI.

EPR Procedure. When the crystal was mounted as represented by Figure 1 several groups of lines characteristic of ^{55}Mn were seen. One of these in the $g_{eff} \approx 4$ region was followed, by successive rotations about the horizontal and vertical axes, to a turning point represented by a maximum value of field; this is labeled E in Figure 2. At this orientation the groups simplified to sextets characteristic of the field along the principal axis of the **D** tensor where only $\Delta M_I = 0$ lines are observed. This orientation is referred to as D_1 on the stereogram of Figure 1.

The same group was followed by trial and error to a low-field turning point, labeled I in Figure 2, a direction in which the characteristic simplification in the spectrum of the loss of $\Delta M_I = \pm 1$ and ± 2 transitions was again observed. This direction coincides with another of the **D**-tensor principal axes and is referred to as D_2.

The third principal axis should be perpendicular to the first two, so the normal to the plane containing D_1 and D_2 was plotted on the stereogram and from it were deduced the horizontal and vertical rotations necessary to bring this direction, D_3, along the field direction. A search was then made for a simplification in the spectrum in the region of this orientation. The $g \approx 4$ group was not sufficiently sensitive for this procedure so attention was transferred to the two groups at higher field, labeled B and C in Figure 2. These two groups move extremely rapidly with changes in orientation and showed strong "forbidden" transitions when only slightly off axis D_3. The best sextet spectrum for group B did not correspond to the best for group C. Finally, an orientation for which a compromise between the best simplification for groups B and C could be achieved was recorded and is shown in Figure 2. This orientation is within 2° of that calculated for D_3 from D_1 and D_2 by using the stereographic net.

For Q-band measurements the crystal was attached with grease to the top of a post mounted axially in a cylindrical cavity operating in the H_{011} mode. The top of the post was cut at 20° from the horizontal and the crystal oriented by eye so that the D_1 axis was as near as possible to the horizontal. Attempts were made to mount the crystal on other specially cut wedges to bring D_2 and D_3 horizontal, but these were not successful.

Results

EPR Data. The X-band spectra along the axes D_1, D_2, and D_3 are shown in Figure 2, and the Q-band spectrum along D_1

Table V. Q-Band (35.550 GHz) Single-Crystal EPR Spectrum of $Zn(Mn)Br_2(OPPh_3)_2$

designation in Figure 3	magnetic field[a] exptl	magnetic field[a] calcd[b]	transition	calcd[b] transition probability
L	2718	2708	$^5/_2$ ($^1/_2$, $-^3/_2$) → $-^5/_2$ ($-^1/_2$)	0.44
M	2858	2928	$^3/_2$, $-^1/_2$ → $^5/_2$ ($^1/_2$, $-^3/_2$)	0.82
N	6073	6057	$^3/_2$, $-^1/_2$ ($-^5/_2$) → $-^3/_2$ ($^5/_2$, $^1/_2$)	2.38
O	7770	*c*	$^5/_2$ ($^3/_2$, $-^1/_2$) → $-^3/_2$ ($^5/_2$, $^1/_2$)	0.0
P	15055	15061	$^5/_2$, $^1/_2$ → $-^1/_2$ ($^3/_2$)	5.07

[a] In Gauss, the magnetic field orientation is $B \| y$. [b] Using data presented in Table VI. [c] Transition not expected when $B \| y$; see text.

Table VI. Spin Hamiltonian Parameters[a] for $Zn(Mn)(OPPh_3)_2Br_2$ and $Zn(Mn)(OPPh_3)_2Cl_2$

	$Zn(Mn)(OPPh_3)_2Br_2$	$Zn(Mn)(OPPh_3)_2Cl_2$[b]
g_x	2.020 ± 0.01	2.03 ± 0.01
g_y	2.019 ± 0.01	2.02 ± 0.01
g_z	2.017 ± 0.01	2.02 ± 0.01
D	0.523 ± 0.01	0.172 ± 0.001
E	0.133 ± 0.001	0.047 ± 0.001
a	+0.002 ± 0.0002	0.006 ± 0.0002
F	−0.00003 ± 0.00001	$<10^{-5}$
D_{xx}	−0.0413	−0.0103
D_{yy}	−0.3073	−0.1043
D_{zz}	+0.3487	+0.1147
A_x	−0.0066 ± 0.0001	−0.0077 ± 0.0005
A_y	−0.0076 ± 0.0001	−0.0079 ± 0.0005
A_z	−0.0076 ± 0.0001	−0.0076 ± 0.0005

[a] Energies are in cm^{-1}. [b] From ref 3.

is shown in Figure 3. The magnetic fields corresponding to the center of each hyperfine sextet labeled A–P are listed in Tables IV and V. Initial assignment of the X-band spectra was by use of **D**/*B* graphs calculated for $S = ^5/_2$,[9] the spin state for high-spin manganese(II). This was followed by refinement assuming the same spin Hamiltonian as for the corresponding chloride[3] and using the program MNES,[3] which gave a best fit to the combined X- and Q-band data with the parameters listed in Table VI. In principle, provided **D** is small enough to use perturbation theory, the sign of **DA** may be found by comparing the mean hyperfine spacings within groups at high and low fields. This method was used for the chloride[3] but fails for the bromide, whose **D** value is too large; depopulation experiments also were ruled out by the use of the two-axis mount. The signs given in Table VI, however, are those required for the best fit of the experimental data with the program MNES assuming a negative value for the hyperfine parameters.

The data in Table VI were also used to produce the energy level plot of Figure 4, which shows the observed transitions for both the X- and the Q-band spectra. The assigned transition for each orientation of the magnetic field and the field value predicted for that transition are given in Tables IV and V; the axes *x*, *y*, and *z* quoted there are the axes of the spin Hamiltonian described previously.[3] The maximum difference between predicted and experimental fields is 2.4%, and most differences are less than 1.0%. The general agreement between predicted and experimental data require the assignment of D_1, D_2, and D_3 to the principal directions of the **D** tensor, D_y, D_z, and D_x, respectively. The angles between pairs of these directions taken from the stereogram are as follows: D_yD_z 87°; D_yD_x 91°; D_xD_z 89°. The discrepancies between these angles and the theoretical 90° are more likely to arise from inaccuracies in the angular measurement than from any fundamental

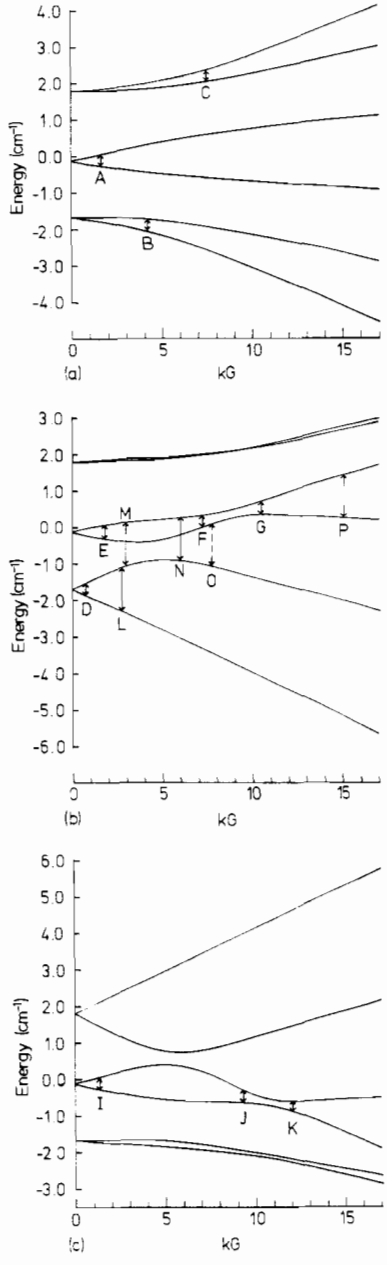

Figure 4. Energy level plots for $Zn(Mn)Br_2(OPPh_3)_2$ calculated with the data of Table VI. a, b, and c represent the field along D_x, D_y, and D_z, respectively. The short arrows represent X-band transitions and the long arrows Q-band transitions. The dashed arrow at O is observed (weakly as in Figure 3) when the field is slightly off axis (see text).

cause; the rotation of the crystal about the horizontal axis is particularly difficult to measure accurately.

The difficulties in obtaining a good spectrum with the field oriented along D_x may be contrasted with the simplicity in the case of the chloride complex[3] for which symmetry requires the spectra from the two molecules in that unit cell to coalesce along *x*, thus making the *x* direction particularly easy to find. For the bromide described here, where there is only one molecule in the unit cell, we based our search for each axis on the nonappearance of the $\Delta M_I = \pm 1, \pm 2$ lines, which are strictly forbidden only when the magnetic field lies along an axis. Calculations using ESRS[3] showed that the transition designated O is strictly forbidden when the field is along the *y* axis but that it becomes allowed by the mixing of some $M_s = ^3/_2, -^1/_2$ into the upper level and rapidly gains intensity with angle as the field moves away from *y*. Its magnitude in Figure 3 relative to those of the other transitions, whose transition

(9) Dowsing, R. D.; Gibson, J. F. *J. Chem. Phys.* **1969**, *50*, 294.

probabilities do not vary rapidly with angle, indicates the crystal to have been about 3° off axis when this spectrum was taken.

Plot of the Molecular Bond Directions. Since we are interested in comparing the EPR **D**-tensor principal directions with molecular bond directions, it is necessary to plot the latter on the stereogram; the procedure adopted to do this was as follows. All coordinates are referred to zinc at the origin, which is assumed to be at the center of the stereogram. The atomic coordinates may be referred to an orthogonal set of axes a^* (the reciprocal axis perpendicular to the bc plane), $b^\dagger$ (perpendicular to both a^* and c), and c by the transformation matrix shown in eq 1. a^* and $b^\dagger$ were generated from a, b, c by their definitions and plotted on the stereogram.

$$\mathbf{R}(\alpha\beta\gamma) = \begin{bmatrix} a\sin\beta\sin\gamma^* & 0.0 & 0.0 \\ -a\sin\beta\cos\gamma^* & b\sin\alpha & 0.0 \\ a\cos\beta & b\cos\alpha & c \end{bmatrix} = \begin{bmatrix} 8.373 & 0.0 & 0.0 \\ -2.385 & 9.082 & 0.0 \\ -5.292 & -4.154 & 11.189 \end{bmatrix} \quad (1)$$

A second transformation is then necessary to refer coordinates in the a^*, $b^\dagger$, c set to the X, Y, Z set of axes. These are orthogonal right-handed sets of axes, and the one may be transformed to the other by the matrix $\mathbf{R}(\Phi\theta\Psi)$, where Φ, θ, and Ψ are the Euler angles for anticlockwise rotations about c, $b^\dagger$, and c again, in that order (eq 2).

$$\mathbf{R}(\Phi\theta\Psi) = \begin{bmatrix} \cos\Phi\cos\theta\cos\Psi - \sin\Phi\sin\Psi & \sin\Phi\cos\theta\cos\Psi + \cos\Phi\sin\Psi & -\sin\theta\cos\Psi \\ -\cos\Phi\cos\theta\sin\Psi - \sin\Phi\cos\Psi & -\sin\Phi\cos\theta\sin\Psi + \cos\Phi\cos\Psi & \sin\theta\sin\Psi \\ \cos\Phi\sin\theta & \sin\Phi\sin\theta & \cos\theta \end{bmatrix} \quad (2)$$

The rotations Φ, θ, and Ψ were estimated from the stereogram as 260, 131.5, and 68°, respectively, which gave the second transformation matrix as shown in eq 2a.

$$\mathbf{R}(\Phi\theta\Psi) = \begin{bmatrix} 0.9562 & 0.0835 & -0.2806 \\ 0.2622 & -0.6701 & 0.6944 \\ -0.1301 & -0.7376 & -0.6626 \end{bmatrix} \quad (2a)$$

The whole process may be represented by eq 3 and 4. The

$$(a^*, b^\dagger, c) = (\mathbf{R}(\alpha\beta\gamma^*))(a, b, c) \quad (3)$$

$$(X, Y, Z) = (\mathbf{R}(\Phi\theta\Psi))(a^*, b^\dagger, c) \quad (4)$$

coordinates of the two oxygen atoms and the two bromine atoms in the X, Y, Z system were then referred to zinc at the origin as vectors, and these directions are also represented in the stereogram of Figure 1. As a check on this procedure the six angles subtended at the zinc atom by all pairs of coordinating ligand atoms (oxygen and bromine) were measured from the stereogram; the maximum deviation from those given in the structure determination was 0.3°.

Discussion

Structures. As can be seen from Table III, the geometric parameters for the two tetrahedra are closely similar. The small differences are probably principally due to the different covalent and van der Waals radii of the bromine and chlorine atoms and to the different packing and site symmetry constraints.

The most striking features of these structures are not the internal comparisons but comparison with the $CuCl_2$[7] and $CuBr_2$[10] analogues. Whereas both the $CuCl_2$ and the $CuBr_2$ complexes have severely distorted tetrahedra with dihedral angles between the OCuO and Cl(Br)CuCl(Br) planes of 72 and 68°, respectively, the $ZnCl_2$ and $ZnBr_2$ arrangements are nearly orthogonal with angles of 88 and 86°, respectively, between these planes. In addition, there are significant differences between the angles made at the Zn and Cu by the halogens. In the $CuCl_2$ and $CuBr_2$ structures the angles were 102 and 104°, respectively, while the values observed in the $ZnCl_2$ and $ZnBr_2$ structures were 117° for both. Among four-coordinate species, a tetrahedral structure is favored on electrostatic and steric grounds while a square-planar structure is preferred according to crystal field stabilization by d^3, d^4, and d^9 complexes, by d^8 high-spin complexes, and by d^5, d^6, d^7, and d^8 low-spin complexes.[11] Weak ligands such as halogens will thus favor the tetrahedron, but since this is Jahn–Teller unstable for a d^9 configuration, the intermediate flattened tetrahedron, which is not infrequently found,[7,10,12-14] is to be anticipated. The zinc(II)[13] and cobalt(II) configurations offer no CFSE preference,[11] and their environments with this type of ligand are more nearly tetrahedral. For both $CoCl_2(OAsPh_3)_2$[15] and $CoCl_2(OPPh_3)_2$[16] the dihedral angle is 88°.

An interesting crystallographic point that emerges from these analyses is the potential danger of assuming isostructurality. The space group for the $ZnCl_2$ and $CuCl_2$ complexes is the same, and the unit-cell parameters are very similar. Additionally, comparison of the intensity sequences in Weissenberg photographs for the $ZnCl_2$ compound with the published data for the $CuCl_2$ compound showed no major differences. This led to the conclusion that the two structures were the same. Only when the major differences were observed in the geometry of the $ZnBr_2$ tetrahedron compared with that reported for the $CuBr_2$ and $CuCl_2$ structures was any seed of doubt sown. Indeed, it is still surprising that such a major perturbation of the structure of the $ZnCl_2$ group can be accommodated without major change in unit cell, space group, or intensity distribution.

Powder EPR Data. There have been many estimates of the zero-field splitting parameters that have been based on powder type EPR spectra; these usually have relied on the observation of high-field features which have been assigned as arising from turning points along the **D**-tensor axes. Wrong assignments may arise with this technique because turning points along the axes do not always give rise to features in the spectrum (the intensity of which depends on the rate at which the resonance field changes with angle) and because sometimes features in the spectrum arise from turning points that are off axis (particularly when **D** is an intermediate or large value). Thus, whenever single crystals are available, the opportunity to check powder data should be taken if only to verify the validity of the earlier work. The compound discussed in this paper is a case in point; an earlier paper[2f] based on a powder spectrum gives a **D** value 20% lower than that quoted here. Comparison of Table IV herein with Table III of the earlier paper establishes that **D** was underestimated largely as a result of assigning the medium-strength bands, at 5150 and 6060 G, to on-axis turning points. Table IV shows that no bands occur in these regions when the field really is directed along the **D**-tensor axes and that the other data of the earlier paper do fit the present interpretation if the above-mentioned features are ignored. However, the error is not serious and certainly has not detracted from the general conclusion that the **D** value of the bromide is considerably greater than that of the chloride

(10) Bertrand, J. A.; Graham, S. L.; Deutsch, H. M.; Van Derveer, D. G. *Inorg. Chim. Acta* **1976**, *19*, 189.
(11) Purcell, K. F.; Kotz, J. C. "Inorganic Chemistry"; W. B. Saunders: Philadelphia, 1977; p 550.
(12) Sager, R. S.; Watson, W. H. *Inorg. Chem.* **1969**, *8*, 308.
(13) Sager, R. S.; Watson, W. H. *Inorg. Chem.* **1968**, *7*, 1358.
(14) de Meester, P.; Skapski, A. C. *J. Chem. Soc., Dalton Trans.* **1973**, 424.
(15) Birker, P. J. M. W. L.; Prick, P.; Beurskens, D. T. *Cryst. Struct. Commun.* **1976**, *5*, 135.
(16) Mangion, M. M.; Smith, R.; Shore, S. G. *Cryst. Struct. Commun.* **1976**, *5*, 493.

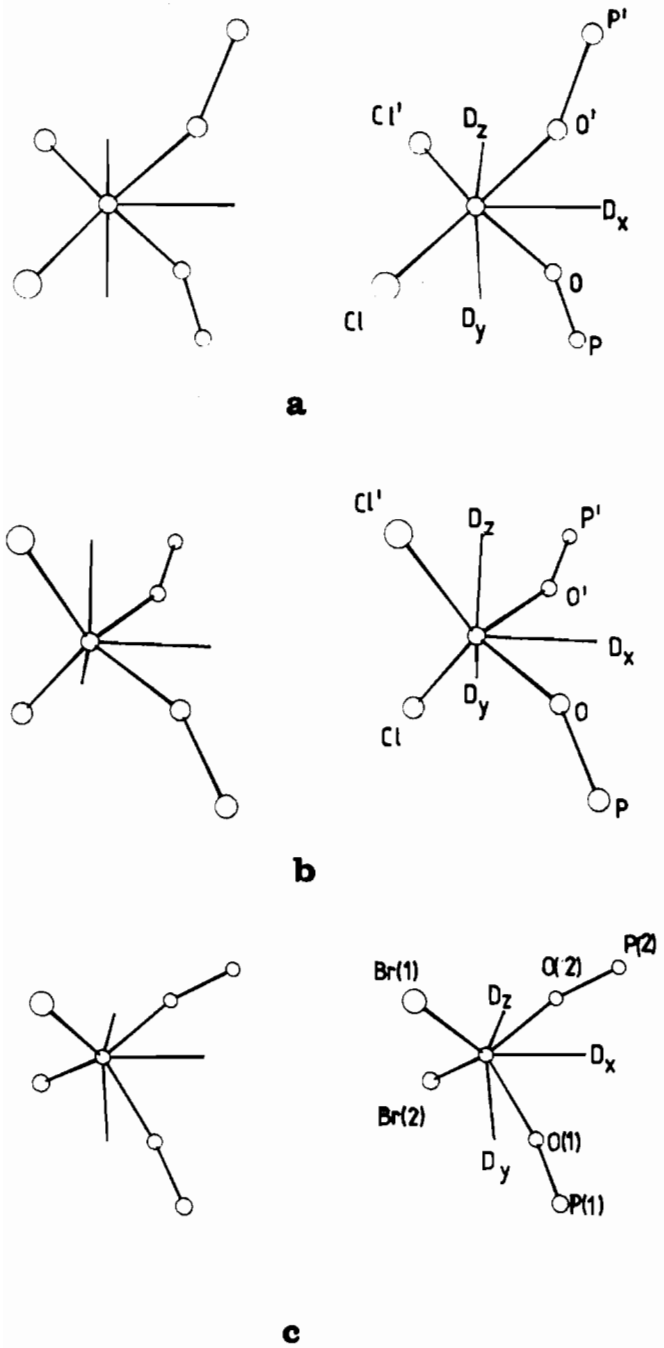

Figure 5. (a and b) Stereoscopic drawings for the two magnetically different zinc tetrahedra in the unit cell of $ZnCl_2(OPPh_3)_2$. The **D**-tensor axes of one Mn(II) ion are superimposed on both tetrahedra. (c) Stereoscopic drawing of the zinc tetrahedron for $ZnBr_2(OPPh_3)_2$ with **D**-tensor axes of Mn(II) ion superimposed.

in these and related compounds[2d] and that that of the iodide is greater still.[2a-c,e,f]

Orientation of D Relative to Ligands. In the earlier paper relating to $Zn(Mn)Cl_2(OPPh_3)_2$[3] there were two magnetically independent molecules in the unit cell but only one direction for D_x which was precisely defined by symmetry requirements, along the ClMnCl′ bisector. There were two measured directions of D_y however (and of D_z) and no obvious way of assigning which **D** tensor belonged to which molecule. Figure 5a,b shows the orientation of the **D** tensor measured earlier for these two nonequivalent molecules, in the chloride structure reported here. With reference to the present results on $Zn(Mn)Br_2(OPPh_3)_2$ we may make a choice between these two orientations for the chloride. Figure 5c gives the orientation of **D** for the bromide where there is no ambiguity because there

Table VII. Angles around D-Tensor Axes in the Mn(II) Tetrahedron

A. Angles between D-Tensor Axes and Selected Molecular Planes

plane	D-tensor axis	angle, deg	plane	D-tensor axis	angle, deg
For $Zn(Mn)Cl_2(OPPh_3)_2$ in Figure 5a					
OMnO′	D_x	0	Cl′MnO′	D_z	26.3
O′MnCl	D_y	38			
For $Zn(Mn)Cl_2(OPPh_3)_2$ in Figure 5b					
OMnO′	D_x	0	Cl′MnO′	D_z	22.9
O′MnCl	D_y	7.1			
For $Zn(Mn)Br_2(OPPh_3)_2$ in Figure 5c					
O(1)MnO(2)	D_x	17.9	O(2)MnBr(1)	D_y	13.8
Br(1)MnBr(2)	D_x	1.2	Br(1)MnO(1)	D_z	13.2
O(1)MnBr(2)	D_y	3.2	Br(2)MnO(2)	D_z	8.4

Two angles are required for each D tensor axis in $Zn(Mn)Br_2(OPPh_3)_2$ due to the asymmetry of the tetrahedron.

B. Angles between D-Tensor Axes and Metal-Ligand Bonds

axis-metal-ligand atom	angle, deg	axis-metal-ligand atom	angle, deg
For $Zn(Mn)Cl_2(OPPh_3)_2$ in Figure 5a			
D_xMnO	48.5	D_yMnO′	41.5
D_xMnO′	48.5	D_yMnCl	89.7
D_xMnCl	58.6	D_zMnCl′	31.5
D_xMnCl′	58.6	D_zMnO′	93.4
For $Zn(Mn)Cl_2(OPPh_3)_2$ in Figure 5b			
D_xMnO	48.5	D_yMnO′	70.5
D_xMnO′	48.5	D_yMnCl	38.9
D_xMnCl	58.6	D_zMnO′	47.0
D_xMnCl′	58.6	D_zMnCl′	71.5
For $Zn(Mn)Br_2(OPPh_3)_2$ in Figure 5c			
D_xMnBr(1)	72.9	D_yMnO(1)	44.9
D_xMnBr(2)	43.5	D_yMnBr(2)	58.8
D_xMnO(1)	57.5	D_zMnBr(1)	54.7
D_xMnO(2)	47.5	D_zMnO(1)	60.5
D_yMnO(2)	67.8	D_zMnBr(2)	64.6
D_yMnBr(1)	44.8	D_zMnO(2)	48.0

is only one molecule in the unit cell. Figure 5a shows D_y and D_z to be close to the OMnO′ and ClMnCl′ planes, respectively. D_z is in fact 93.4 and 86.6°, respectively, to the two metal–oxygen bonds, requiring that D_y is within 3.4° of the OMnO′ plane. Similarly, D_y is placed 89.7 and 90.3° from the metal–chlorine bonds, requiring that D_z is within 0.3° of the ClMnCl′ plane.

The orientation of **D** in the bromide is quite different from this as may be seen in Figure 5c, which shows D_y and D_z to be well away from the O(1)MnO(2) and Br(1)MnBr(2) planes, respectively; rather, these two directions are in the O(1)MnBr(2) and O(2)MnBr(2) planes, respectively (see also Figure 1). Figure 5b shows a close correspondence to Figure 5c in this respect, D_y and D_z being closer to the O′MnCl and O′MnCl′ planes. The data in Table VII may be used to confirm this statement. Thus, if the major factors that determine the magnitude and direction of the **D** tensors are similar in these two molecules, then Figure 5b is more likely to represent the **D**-tensor orientation in $Zn(Mn)Cl_2(OPPh_3)_2$ than Figure 5a. We note in passing that Bencini et al.[17] made the other choice with reference to cobalt-doped $ZnCl_2(OPPh_3)_2$; they quote effective g values whose orientations would be determined by **D** in that d^7, $S = {}^3/_2$ system which assumes an effective $S' = {}^1/_2$.

Dependence of D on Covalence. The theoretical interpretation of the magnitude and sign of **D** is a complex matter with

(17) Bencini, A.; Benelli, C.; Gatteschi, D.; Zanchini, C. *Inorg. Chem.* **1979**, *18*, 2137.

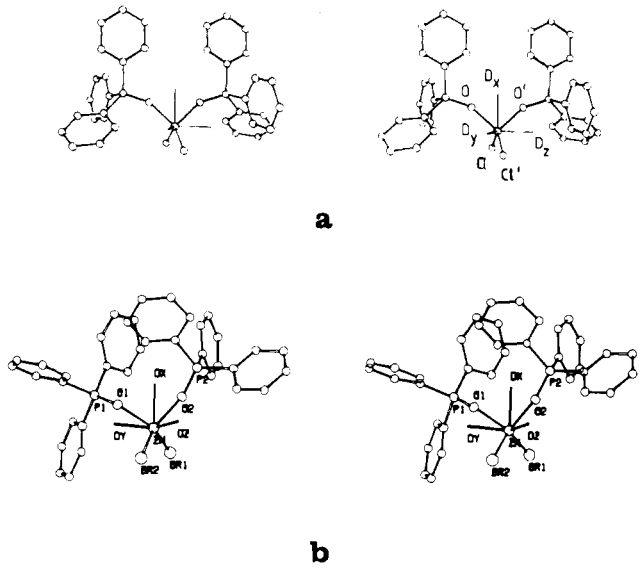

Figure 6. (a) Stereoscopic drawing of $ZnCl_2(OPPh_3)_2$ with **D**-tensor axes of Mn(II) superimposed. (b) Stereoscopic drawing of $ZnBr_2(OPPh_3)_2$ with **D**-tensor axes of Mn(II) superimposed.

contributions arising at least in principle from sums of electrostatic point charges, polarization dipoles, relativistic term overlap, and covalence and lattice vibrations.[18] Sometimes small values of **D** result from relatively large terms which have opposite sign, and in these cases the actual value is critically dependent on the symmetry and strength of the crystal field at the paramagnetic ion.[2g] However, the relatively large value we find in this compound and the fact that it increases in the order Cl < Br < I[2f,3] imply that, even though there may be opposing mechanisms, at least one mechanism is very strong and increasing in this order. Venoyama and Sakai[19] similarly found **D** in some porphyrin halides to increase with the same order of ligands and noted inverse proportionality with the Pauling electronegativities of these halide ions. From the definition of electronegativity by Pauling we infer therefore that **D** in these ferric porphyrin halides is increasing as the ionic contribution to the molecular wave function decreases or that **D** increases as covalence increases. The effect has been observed before with Eu^{2+} [20] and with Mn^{2+}, where the zero-field splitting parameter increased as a function of temperature while the metal hfs decreased.[21] However, in the latter case, in which Mn^{2+} was doped into $Ca(OH)_2$ and $Ca(OD)_2$, a strong isotope effect was seen for the zero-field splitting but not for A_{iso}, implying different mechanisms operated to determine these two parameters. But these were small effects relative to the magnitude of **D** we report here. There seems little doubt that covalence must be important in determining **D**. Note from Figure 1 and Table VII that all three principal values of **D** lie in or close to the planes defined by the bond directions and are close to the bisectors of the angles between these bond directions. We expect this on the basis that the initially spherical 3d electron cloud on a free ion of manganese(II) will distort so as to avoid regions of high electron density as ligands approach, i.e., along the C_2 rotation axes in the case of a tetrahedron. We argue that the negatively charged halogens will strongly repel the Mn(II) d electrons and so direct the D_z direction of the **D** tensor (largest positive value) to be normal to the XMnX bisector (X = Br or Cl) and in the OMnO plane. On the other hand, the electronegative oxygen atoms will direct D_z to be normal to the OMnO bisector (which is almost coincident with the Br(1)MnBr(2) bisector and exactly coincident with that of ClMnCl) but in the XMnX plane. The sum of these two effects (if approximately equal) would be to place D_z along an intermediate direction, i.e., close to an OMnX bisector. The direction of least distortion (D_x) will reasonably be the direction of the opposing halogen and oxygen repulsive forces (i.e., XMnX bisector). Thus, D_y (being normal to D_z and D_x) will also be close to an OMnX bisector. D_y (the largest negative value of the **D** tensor) is the direction that is least effective in avoiding electron density, while D_z is the most effective. In the case of the chloride, the most electron-dense region would be around a chlorine atom and it may be noted in Table VII that the angle D_yMnCl < D_zMnCl in keeping with this observation. The bromine atom in the bromide, however, being less electronegative, will have a weaker directing effect as may be observed from the angles in Table VII. Furthermore, since it is more strongly covalent than chlorine, it will release electrons more effectively to the Mn(II) 3d shell (both σ and π bonding), which in turn will be more strongly distorted, giving rise to the higher **D** value that is observed. It is also to be noted from Table VI that the lower hyperfine parameters for the bromide are consistent with increased covalency particularly along the x direction, which approximately bisects the metal–halogen interbond angle.

It is always possible that atoms more distant than the nearest neighbors may contribute to the magnitude and orientation of **D**, and for this reason we have examined the possible effects of the phenyl groups in these molecules. It is rather strikingly seen in the stereoscopic drawings of the chloride (Figure 6a) that D_x, D_y, and D_z successfully avoid the π-electron density of the phenyl groups, which are therefore presumably unimportant in determining **D**. But in the case of the bromide (Figure 6b), although D_x clearly finds an annular space between three phenyl groups, D_y and D_z do seem to be oriented toward phenyl groups. D_z is directed toward the nodal planes of two of them (zero π density) while D_y is directed over the face of one of them (maximum π density). Thus, it appears that in highly covalent molecules such as these, although the orientation of the **D** tensor is determined predominantly by nearest neighbors to the manganese atom, other groups in the molecule or even on neighboring molecules may well be significant. It would be interesting to apply the superposition model[22] for determining **D** to this molecule, but at present there are insufficient data.

Acknowledgment. Charles Kosky wishes to thank Manhattan Community College for a Faculty Fellowship.

Registry No. $ZnCl_2(OPPh_3)_2$, 14494-88-3; $ZnBr_2(OPPh_3)_2$, 14552-78-4; Mn, 7439-96-5.

Supplementary Material Available: Tables of bond lengths and angles, hydrogen atom coordinates, and anisotropic thermal parameters for $ZnCl_2(OPPh_3)_2$ and $ZnBr_2(OPPh_3)_2$ (5 pages). Ordering information is given on any current masthead page.

(18) (a) Blume, M.; Orbach, R. *Phys. Rev.* **1962**, *127*, 1587. (b) Sharma, R. R.; Das, T. P.; Orbach, R. *Ibid.* **1966**, *149*, 257; **1967**, *155*, 338. (c) Wybourne, B. G. *J. Chem. Phys.* **1965**, *43*, 4506. (d) van Heuvlen, A. *Ibid.* **1967**, *46*, 4903. (e) Stager, C. V. *Can. J. Phys.* **1968**, *46*, 807. (f) Folen, V. J. *Phys. Rev. B: Solid State* **1973**, *7*, 2771. (g) Narayana, P. A. *Ibid.* **1974**, *10*, 2676. (h) Novák, P.; Veltroský, I. *Phys. Status Solidi B* **1976**, *73*, 575. (i) Rispin, A. S.; Sato, M.; Kon, H. *Theor. Chim. Acta* **1978**, *50*, 95. (j) Leblé, A.; Rousseau, J. J.; Fayet, J. C. *J. Phys. Chem. Solids* **1979**, *40*, 1065.

(19) Venoyama, H.; Sakai, K. *Spectrochim. Acta, Part A* **1975**, *31A*, 1517.

(20) Nicollin, D.; Bill, H. *J. Phys. C* **1978**, *11*, 4803.

(21) Holluj, F.; Kwan, C. T. *Phys. Rev. B: Solid State* **1974**, *9*, 3673.

(22) Newman, D. J.; Urban, W. *Adv. Phys.* **1975**, *24*, 793.